Int. J. Electron. Commun. (AEÜ) 104 (2019) 91–98

Contents lists available at ScienceDirect

International Journal of Electronics and Communications (AEÜ)

journal homepage: www.elsevier.com/locate/aeue

Regular paper

Numerical analysis of SAR and temperature distribution in two dimensional human head model based on FDTD parameters and the polarization of electromagnetic wave

Z.M. Lwin [a,*], M. Yokota [b]

[a] Interdisciplinary Graduate School of Agriculture and Engineering, University of Miyazaki, 1-1 Gakuen Kibanadai Nishi, Miyazaki 889-2192, Japan
[b] Department of Electrical and Systems Engineering, University of Miyazaki, 1-1 Gakuen Kibanadai Nishi, Miyazaki 889-2192, Japan

ARTICLE INFO

Article history:
Received 11 November 2018
Accepted 20 March 2019

Keywords:
FDTD
Transverse magnetic
Transverse electric
Human head

ABSTRACT

In the modern environment, electromagnetic waves from various types of transmission antennas, such as those in cell phones are propagating around the human body. The electromagnetic (EM) wave is absorbed by the human body and some undesirable effects occur in the tissues. The specific absorption rate (SAR) is a useful parameter for measuring these effects. In this study, changes in human body temperature, considered as thermal effects, are computed in a tissue-based analysis of the SAR. The finite difference time domain (FDTD) method and the bio-heat equation are used primarily to calculate the consequent effects. Two-dimensional formulation of FDTD is applied in the computing, and the propagation of the electric field is investigated in two polarizations: transverse electric (TE) wave, and transverse magnetic (TM) wave. The electric field source is kept near the human head which is designed as structured layers.

1. Introduction

In modern society, a smartphone is an essential device for people so the electromagnetic wave radiation to the human body is an interesting research area. Thus, researchers try to measure the radiation effect of the cell phone antenna on human beings. The specific absorption rate (SAR) is a useful parameter for measuring these exposures. Some researchers use a specific device (thermal imaging camera) to measure the body temperature changes from which the SAR value is calculated as a result of the cell phone usage [1]. On the other hand, most studies first computed the SAR result, from which the temperature rise is consequently derived [2–9].

Some researches use a complex-structured human body model from well-known associations, such as the National Institute of Information and Communications Technology (NICT), and the radiation effects are analyzed using special commercial software such as COMSOL™ [2,3]. Magnetic resonance imaging (MRI) based human body models are popular in the numerical analysis area of electromagnetic wave radiation research [2,4,5]. Some other researches use a simple design of the human model, such as a cylindrical or spherical shape, for the numerical analysis [6–10].

In a study by Siriwitpreecha et al., a two-dimensional human body model was examined in both transverse electric (TE) and transverse magnetic (TM) waves using the finite element method (FEM) [2]. MRI based 2D slices of a human body model were used to compute the SAR and temperature increase due to leakage electromagnetic waves of 300 MHz, 915 MHz, 1300 MHz, and 2450 MHz. Using an MRI image, the nine layers of the human model were analyzed, and the results were validated with a simple three-layered elliptical human body model. The three-dimensional approach takes considerable time and consumes much memory space. Thus, the two-dimensional approach is used to measure the absorption rate for faster computation times and lower hardware cost. There are some earlier researches on the two-dimensional approach. Vaquer et al. [6] studied the electromagnetic radiation effects on the dielectric cylinder model in two dimensional TM and TE polarized cases. They used the fast-Fourier-transform conjugate gradient method (FFT-CGM), and the maximum SAR value as a result of scattering the wave at a 3 cm distance from the ear was measured at 1.89 GHz. Takafumi Ohishi et al. [7] studied the biological effect of plane wave propagation in TM and TE waves on a two-dimensional three-layered elliptical human model using numerical analysis. The FDTD method and the perfectly matched layer (PML) absorbing boundary were applied to compute the electric field. Furthermore, the SAR value for different angle-of-incidence to the human body was investi-

* Corresponding author.
E-mail addresses: zinmarlwin82@gmail.com (Z.M. Lwin), m.yokota@m.ieice.org (M. Yokota).

https://doi.org/10.1016/j.aeue.2019.03.010
1434-8411/

gated at frequencies ranging from 300 MHz to 1.8 GHz, and the maximum SAR was determined from the frontal incidence. They concluded that the average SAR value for TE wave incidence is higher than that for TM waves at all frequencies except 300 MHz. Nishizawa et al. [8] used the method of moment (MoM) to determine the SAR value in a three-layered elliptical human body model radiated by a plane-wave source. Alisoy et al. [9] used the two-dimensional FDTD method with the TM wave to investigate the SAR value in rectangular-shaped three-layered human tissue with an air interface. They simulated the biomedical device as a point source kept not only near the body but also inside human skin and fat. The propagation characteristics were presented using the reflection properties of the electromagnetic wave in human tissue layers. Kamalaveni et al. [18] studied SAR measurements and temperature rise in the human head using FEM and the bio-heat equation, and also presented a way to reduce these unwanted effects.

In this study, a simple circular-shaped of a two-dimensional human head was designed to compute the SAR. It is generally known that different people have different head size and that the thickness of each tissue layer would rarely be the same length. The motivation for using the simple numerical model is to obtain general information on the specific tissues affected by radiation. One of the well-known numerical methods, FDTD, was used in this study. For two-dimensional FDTD, most other researchers apply only the TM wave approach. In contrast, we calculated and compared the results for the TM wave and TE wave. For the temperature calculation, we applied the two-dimensional based bio-heat equation with FDTD discretization, while other studies use three-dimensional and one-dimensional approaches [3,14]. The comparison of the SAR results dependent on the FDTD parameters was also analyzed. The temperature rise under long-term exposure was also studied and is discussed in the results. The line source radiation of the two-dimensional approach in near-field studies has two different polarizations: E polarization (TM wave) and H polarization (TE wave). Using the FDTD method, Mur absorbing boundary was applied to derive the electric field intensity value. The human head was structured in a six-layered circular cylindrical model. The frequencies investigated were 3.35 GHz and 4.5 GHz, which are assuming of the 5G frequencies.

2. Methods

FDTD is the Maxwell equation based numerical approach [11]. The two-dimensional calculation of FDTD has two polarizations corresponding to the TM wave and TE wave. The computation domain of the FDTD is bordered with Mur's first absorption boundary method. The SAR calculation procedure for each method is also presented in this section. In both cases, the analysis is done using the sinusoidal incident wave. The amplitude of the incident electric field changes depending on the transmission power of the antenna.

2.1. TM wave

To derive the updated equation for the TM wave, we much consider its three components one electric field and two magnetic fields (Ez, Hx, Hy). The TM wave sets up the electric field transverse to the z-axis, and it is referred to as E polarization of the wave. The electric field is primarily determined using the Maxwell equation [12], as in Eqs. (1)–(3) based on permeability μ, permittivity ε and conductivity σ of the specific material.

$$\frac{\partial \mathrm{E_z}}{\partial \mathrm{y}} = -\mu \frac{\partial \mathrm{H_x}}{\partial \mathrm{t}} \tag{1}$$

$$\frac{\partial \mathrm{E_z}}{\partial \mathrm{x}} = \mu \frac{\partial \mathrm{H_y}}{\partial \mathrm{t}} \tag{2}$$

$$\frac{\partial \mathrm{H_y}}{\partial \mathrm{x}} - \frac{\partial \mathrm{H_x}}{\partial \mathrm{y}} = \varepsilon \frac{\partial \mathrm{E_z}}{\partial \mathrm{t}} + \sigma \mathrm{E_z} \tag{3}$$

These equations can be simplified in terms of finite difference notation and also substituted with the time and space of lattice, with n for time and (i,j) for the two-dimensional lattice point in Eqs. (4)–(6) [11].

$$H_x^{n+\frac{1}{2}}(i,j) = H_x^{n-\frac{1}{2}}(i,j) - \frac{1}{\mu}\frac{\Delta t}{\Delta y}[E_z^n(i,j+1) - E_z^n(i,j)] \tag{4}$$

$$H_y^{n+\frac{1}{2}}(i,j) = H_y^{n-\frac{1}{2}}(i,j) + \frac{1}{\mu}\frac{\Delta t}{\Delta x}[E_z^n(i+1,j) - E_z^n(i,j)] \tag{5}$$

$$E_z^{n+1}(i,j) = \frac{\left(1-\frac{\sigma\Delta t}{2\varepsilon}\right)}{\left(1+\frac{\sigma\Delta t}{2\varepsilon}\right)} E_z^n(i,j) + \frac{\frac{\Delta t}{\varepsilon}}{\left(1+\frac{\sigma\Delta t}{2\varepsilon}\right)\Delta x}[H_y^{n-\frac{1}{2}}(\mathrm{i},\mathrm{j}) - H_y^{n-\frac{1}{2}}(\mathrm{i}-1,\mathrm{j})] - \frac{\frac{\Delta t}{\varepsilon}}{\left(1+\frac{\sigma\Delta t}{2\varepsilon}\right)\Delta y}[H_x^{n+\frac{1}{2}}(\mathrm{i},\mathrm{j}) - H_x^{n-\frac{1}{2}}(\mathrm{i},\mathrm{j}-1)] \tag{6}$$

where $\Delta x, \Delta y$ and Δt are fundamental FDTD parameters. Δx and Δy are the horizontal and vertical direction of the grid or cell size of the FDTD cells. In this study, we used the square grid $(\Delta x = \Delta y)$. Δt is the time step for the propagation of the wave.

SAR is a function of conductivity, electric field, and tissue density ρ [12]. SAR can be calculated using the following equation:

$$\mathrm{SAR} = \frac{\sigma \mathrm{Ez}^2}{2\rho} \quad [\mathrm{W/kg}] \tag{7}$$

The peak of the electric field (Ez) of the TM wave resulting from the FDTD iteration is applied to the SAR calculation.

2.2. TE wave

To derive the updated equation for the TE wave, we must consider its components. It also has three components, but opposite in composition to the TM wave: two electric fields and one magnetic field (Hz, Ex, Ey). Maxwell's curl equation is applied as in Eqs. (8)–(10) [12]. The TE wave sets up the magnetic field transverse to the long (z-axis) of the structure and it is referred to as H polarization.

$$\frac{\partial E_y}{\partial x} - \frac{\partial E_x}{\partial y} = -\mu \frac{\partial H_z}{\partial t} \tag{8}$$

$$\frac{\partial E_x}{\partial t} = \frac{1}{\varepsilon}\left[\frac{\partial H_z}{\partial x} - \sigma E_x\right] \tag{9}$$

$$\frac{\partial E_y}{\partial t} = \frac{1}{\varepsilon}\left[-\frac{\partial H_z}{\partial y} - \sigma E_y\right] \tag{10}$$

Similar to the TM wave, the simplified version of the TE wave Maxwell's equation is derived as the following using finite difference terms and grid index [11]:

$$H_z^{n+\frac{1}{2}}(i,j) = H_z^{n-\frac{1}{2}}(i,j) + \frac{\Delta t}{\mu}\left[\frac{E_y^n(i,j) - E_y^n(i-1,j)}{\Delta y} - \frac{E_x^n(i,j) - E_x^n(i,j-1)}{\Delta x}\right] \tag{11}$$

$$E_x^{n+1}(i,j) = \frac{1-\frac{\sigma\Delta t}{2\varepsilon}}{1+\frac{\sigma\Delta t}{2\varepsilon}} E_x^n(i,j) + \frac{\frac{\Delta t}{\varepsilon}}{1+\frac{\sigma\Delta t}{2\varepsilon}}\left[\frac{H_z^{n+\frac{1}{2}}(i,j) - H_z^{n-\frac{1}{2}}(i,j-1)}{\Delta y}\right] \tag{12}$$

$$E_y^{n+1}(i,j) = \frac{1-\frac{\sigma\Delta t}{2\varepsilon}}{1+\frac{\sigma\Delta t}{2\varepsilon}} E_y^n(i,j) - \frac{\frac{\Delta t}{\varepsilon}}{1+\frac{\sigma\Delta t}{2\varepsilon}}\left[\frac{H_z^{n+\frac{1}{2}}(i,j) - H_z^{n-\frac{1}{2}}(i-1,j)}{\Delta x}\right] \tag{13}$$

having two electric components give the SAR equation as Eq. (14). The intensity of the two electric fields of the TE wave is calculated as $E_{TE} = \sqrt{E_x^2 + E_y^2}$ for the SAR equation.

$$SAR = \frac{\sigma (E_{TE})^2}{2\rho} \quad [W/kg] \tag{14}$$

2.3. Temperature calculation

When the human head is exposed to the region of electromagnetic wave propagation, the thermal effects of EM wave radiation occur. The bio-heat equation computes the thermal effects using heat conduction, blood flow, and blood temperature to calculate the temperature rise in the human body [4]. The bio-heat equation is as follows [4]:

$$C_p \rho \frac{\partial T}{\partial t} = K \nabla^2 T + \rho SAR - b(T - T_b) \tag{15}$$

and its boundary condition is

$$K \frac{\partial T}{\partial n} = -h(T - T_a) \tag{16}$$

where $T = T(x, y, t)$ in two-dimensional case is temperature (°C) at time t, C_p is the specific heat (J/kg°C), K is the thermal conductivity (W/m°C), b is the constant (W/m^3°C) related to blood flow, T_b is blood temperature, T_a is the ambient temperature, n is the unit vector normal to the surface of the head, and h is the heat transfer coefficient (W/m^2°C). SAR is calculated from the FDTD. The bio-heat equation of the finite-difference approximation in 2D format is as follows:

$$T_{(i,j)}^{m+1} = T_{(i,j)}^{m} + \frac{\Delta t SAR_{(i,j)}}{C_{p_{(i,j)}}} - \frac{\Delta t b_{(i,j)}}{C_{p_{(i,j)}} \rho_{(i,j)}} \left(T_{(i,j)}^{m} - T_b \right) + \frac{\Delta t K_{(i,j)}}{\Delta^2 C_{p_{(i,j)}} \rho_{(i,j)}} \left[T_{(i+1,j)}^{m} + T_{(i-1,j)}^{m} + T_{(i,j+1)}^{m} + T_{(i,j-1)}^{m} - 4T_{(i,j)}^{m} \right] \tag{17}$$

$$T^*(i_{min}, j) = \frac{K T^*(i_{min} + 1, j)}{K + h\Delta} + \frac{T_a h \Delta}{K + h\Delta} \tag{18}$$

In Eq. (17), $\Delta^2$is the cell size of the square grid in the space of heat transfer ($\Delta^2 = \Delta x * \Delta y$), while Δx and Δy are the same as the cell size of the FDTD grid. Eq. (18) is for the x-direction of heat transfer ($\Delta = \Delta x$). Eq. (17) is used to calculate the temperature changes inside of the human head and Eq. (18) is for temperature calculations for the skin surface. Similar approximations can be done for the y-direction. Time step Δt in the heat equation is not the same as the time step Δt in the FDTD [4]. For numerical stability, Δt in the heat equation is calculated as follows [4]:

$$\Delta t \leq \frac{2\rho C_p \Delta^2}{12K + b\Delta^2} \tag{19}$$

where C_p, K, and b are assumed as constants because the heating effect on human tissue is small.

Air temperature (T_a) and blood temperature are assumed as 25 °C and 37 °C respectively. The heat transfer coefficient (h) is set as 10.5 (W/m^2°C) [3]. The constants of the bio-heat equation are presented in Table 1.

3. Modeling

The human head was modeled as six different layers: skin, fat, bone, dura, CSF (cerebrospinal fluid), and brain. Each layer has different dielectric properties, and these values depend on the frequency. The dielectric permittivity and conductivity of human tissues at the frequencies of 3.35 GHz and 4.5 GHz, and the thickness of the tissues are presented in Table 2. The dielectric properties of the tissues are sourced from an online database [13].

Table 1
Thermal parameters of tissues [4].

Tissue	C_p(J/kg°C)	K (W/m°C)	B (W/m^3°C)	ρ(Kg/m^3)
Skin	3600	0.42	9100	1010
Fat	3000	0.25	1700	920
Bone	3100	0.39	3300	1810
Dura	3600	0.5	9100	1010
CSF	4000	0.62	0	1010
Brain	3650	0.535	40,000	1040

Table 2
Dielectric properties of tissues.

	3.35 GHz		4.5 GHz		Thickness
Layer	σ (S/m)	ε	σ (S/m)	ε	(mm)
Skin	1.9363	37.14	2.6861	36.18	1
Fat	0.1477	5.189	0.2119	5.0766	1.4
Bone	0.5815	10.87	0.8438	10.28	4.1
Dura	2.2569	40.9	3.1523	39.477	0.5
CSF	4.3952	64.83	5.8729	62.854	2
Brain	2.1121	41.34	3.0332	39.91	162

The geometrical presentation of the head model and transmission source are shown as a color map and diagram in Fig. 1(a) and (b), respectively. Calculation area for the FDTD is 30 cm square. In Fig. 1(a), the wide blue area is free space and the yellow mark represents the source. The circle with colorful layers represents each tissue layer. The outermost cyan color layer represents skin, blue represents fat, light blue represents bone, green represents dura, yellow represents CSF and the innermost green layer represents the brain. The line L is the cross-sectional line of the head and the SAR in that line is discussed in subsequent sections. The radius of the human head is assumed as 9 cm in Fig. 1(b) which is the diagram of the coaxial cylindrical head model and a cell phone.

4. Comparison of absorption rate with the grid point of the wavelength

For numerical computation using the FDTD method, the grid resolution is one of the important factors because it can influence the computational SAR results. The grid resolution is related to the cell size Δx and Δy. The cell size in x and y direction is defined by $\Delta x = \frac{\lambda_{min}}{N_\lambda}$ where $\Delta x = \Delta y$. The grid resolution or the grid point N_λ is the number of points per minimum wavelength λ_{min}. λ_{min} is computed from $\lambda_{min} = \frac{c_0}{f_{max} n_{max}}$ where n_{max} is the maximum refractive index, f_{max} is the maximum frequency, and c_0 is the speed of light in free space. The n_{max} is computed from the highest relative permittivity ε_r of the tissue layers using $n_{max} = \sqrt{\varepsilon_r}$. Among the six types of tissues, CSF has the highest relative permittivity. N_λ is chosen according to the material which the electromagnetic wave passes through. The temporal time steps Δt of the FDTD depend on the cell size of the FDTD and can be derived from $\Delta t = 0.9 / \left(c_0 \times \sqrt{\frac{1}{\Delta x^2} + \frac{1}{\Delta y^2}} \right)$. Computation of Δt has to follow the Courant stability condition. Fig. 2 shows the comparison of SAR on line L for the different N_λ. It may be inferred that the small number of points leads to the higher SAR results, and choosing the appropriate number of grid points is also important for computing with the FDTD method. Fig. 2 presents the results of the TM wave propagation to the head at 3.35 GHz from an 0.125 W transmitting source located 1 cm away from the head.

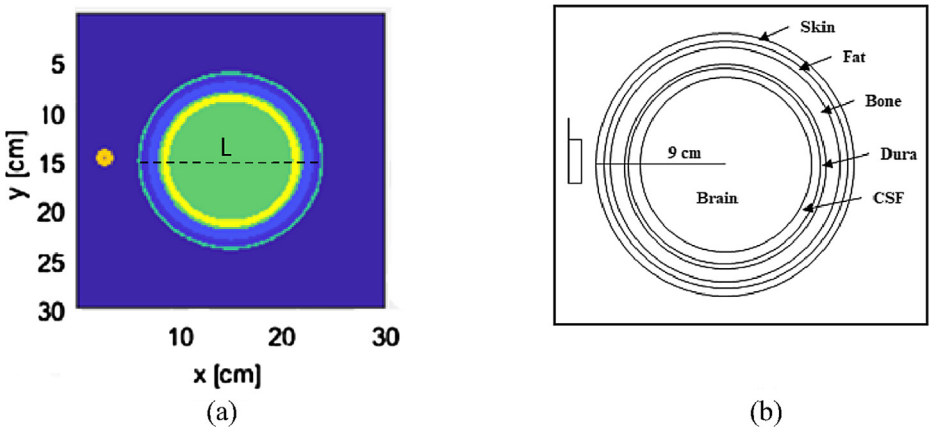

Fig. 1. Geometry of the calculation model: (a) color map and (b) diagram. (For interpretation of the references to colour in this figure legend, the reader is referred to the web version of this article.)

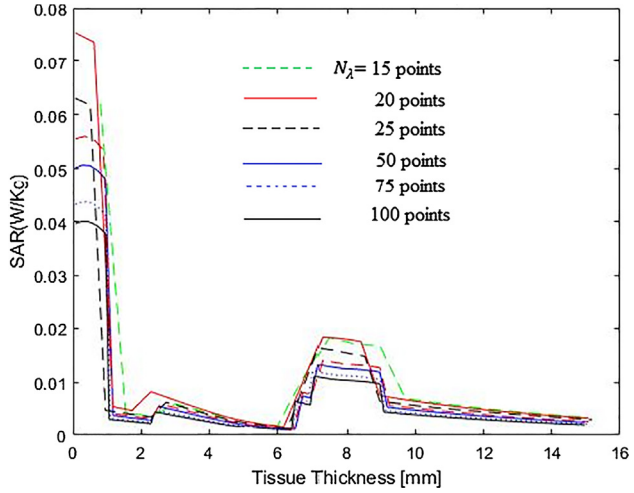

Fig. 2. Comparison of SAR at different grid resolution points.

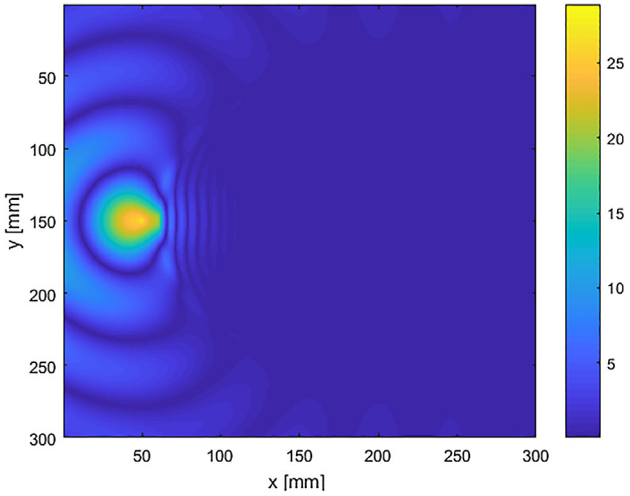

Fig. 3. Distribution of the electric field at 3.35 GHz.

The grid resolution points N_λ per minimum wavelength are chosen as 15, 20, 25, 50, 75 and 100 points that give 0.7, 0.56, 0.44, 0.22, 0.15, and 0.11 mm cell sizes, respectively. The wider the cell size it uses, the lower the number of cells it gets in the FDTD two dimensional array. At that point, although the execution time is fast because of the large FDTD cell size, it is difficult to get a smooth result. For example, for grid point 15 and 20, with FDTD cell size 0.7 mm and 0.56 mm, the cell size is greater than the thinnest dura tissue layer with 0.5 mm thickness. Thus, it is impossible to obtain information on that layer. The grid points greater than 50 points have very small cell size and a large cell array. Consequently, it has much longer processing time in computation. In this study, 25 points grid resolution is chosen to analyze the SAR results because it has the appropriate cell size of 0.44 mm and its results are not much different from the results for 50 points. The validation for choosing 25 points is presented in the following section.

5. Distribution of the electric field and SAR

The propagation of the electric field from a 1 cm distant source to the human head by an incident transmission antenna with a power of 1 W is presented in Fig. 3. It uses a grid resolution of 25 points over the minimum wavelength on the 3.35 GHz frequency. The FDTD cell size of 0.44 mm and the temporal time-step of 0.94 ps are simulated for a maximum of 8527 FDTD iterations. These results are for the 8 ns exposure. The small electric field can be transmitted to the inside of the human head. To prevent reflection from the boundary and thus obtain accurate results, Mur absorption boundary is used and is presented in Fig. 3.

SAR distribution inside the human head can be seen clearly via the logarithmic values of the SAR presented in a color map in Fig. 4. The SAR value in yellow color is the highest rate which is found in the part of the head near the electric field transmission source. The cross-sectional view in Fig. 5 highlights the location of the tissue layers in the SAR distribution. The SAR reaches its peak at Skin and CSF layers, which have a high permittivity rate, and these results are in good agreement with previous studies [9,14,15]. In the fat and bone layer, the SAR suddenly and significantly decreases. The SAR reaches almost zero inside the brain at points farthest from the source.

6. Local SAR of different polarizations at 3.35 GHz and 4.5 GHz

Although the behavior of the SAR distribution in each tissues layer is similar, the rate of the induced SAR in the TE wave in Fig. 7 is much higher than that in the TM wave in Fig. 6. This is due to the different propagation characteristics of the wave in parallel

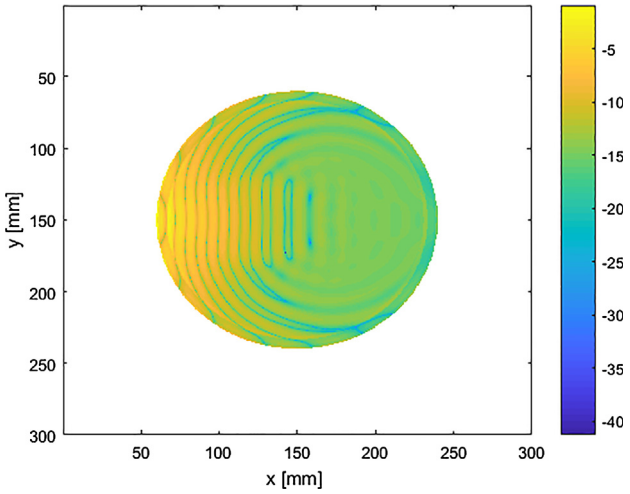

Fig. 4. Distribution of SAR in logarithmic view.

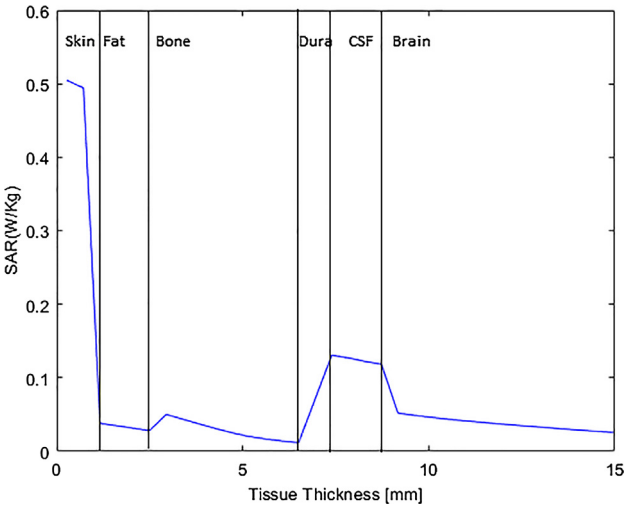

Fig. 5. Distribution of SAR in six-layered tissue.

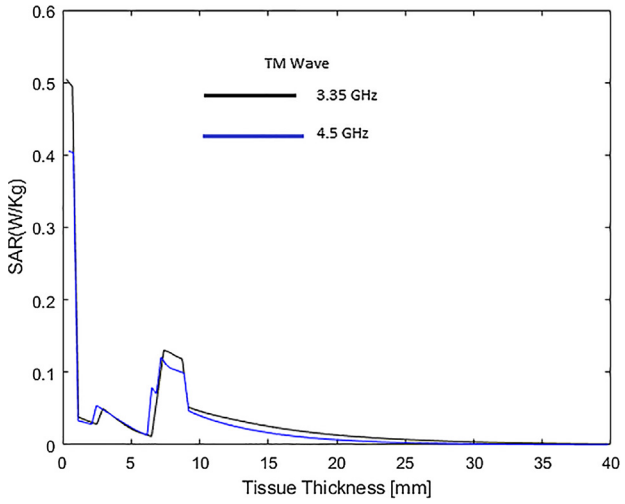

Fig. 6. SAR distribution in the TM wave.

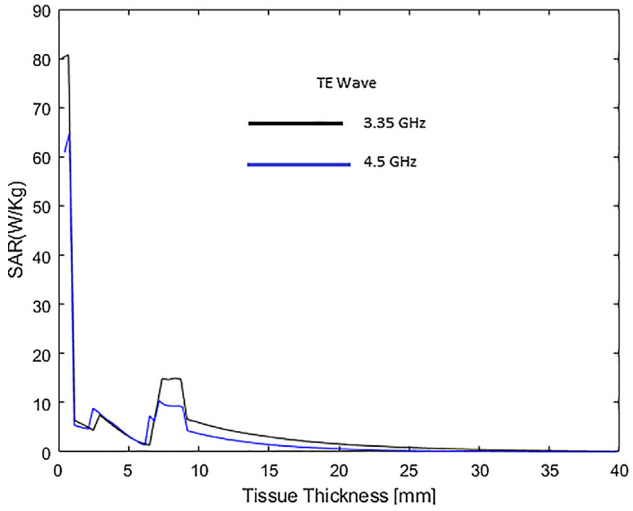

Fig. 7. SAR distribution in the TE wave.

and perpendicular polarization. In the TM wave, the electric field line is parallel to the propagation of the wave while the electric fields in the TE wave are perpendicular to the wave direction. As explained in section 3, the TE wave has two electric fields and a magnetic field transverse to the propagation of the waves. Thus, the two electric fields propagate around the human head and this creates a large absorption area on the head. In this way, the absorption rate is higher than with the TM wave. This is called the diffraction phenomenon of wave propagation. Figs. 6 and 7 present the SAR results at 1 W incident power, 1 cm distance between the human head and the cell phone, with 25 points of grid resolution. From the frequency based information on the TM wave in Fig. 6, the absorption rate at 3.35 GHz frequency is higher than at 4.5 GHz, in the skin, CSF layer, and brain. However, the difference between the SAR at the two frequencies is slight in Fat and Bone layers. For the frequency based information on the TE wave in Fig. 7, although the absorption rate at the 4.5 GHz frequency is higher than that at 3.35 GHz in the outermost three layers, the penetration rate of the 3.35 GHz is stronger and it can reach farther into the brain region. For both frequencies, the SAR rate in TE wave is higher than in the TM wave, and this is in good agreement with the results of a previous study [6].

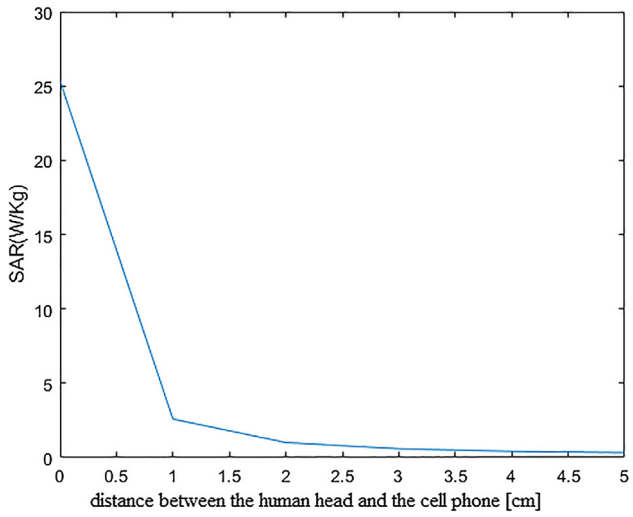

Fig. 8. Comparison of SAR with the distance of the antenna from the skin layer.

7. Comparison of the absorption rate with the position and incident power of the antenna

The results from Fig. 8 shows that the maximum SAR value in the skin layer depends on the distance between the human head and the cell phone at a 2 W transmission power on 3.35 GHz. That result has a good agreement with previous research [15]. The longer distance leads to the reduction of SAR inside the tissue. If we use the cell phone at a distance less than 1.5 cm from the human body, the SAR is greater than the minimum limiting threshold for SAR (2 W/Kg) according to the guidelines [16,17].

The transmission power of the cell phone antenna is between 0.1 W and 2 W. The antenna from the cell phone emits electromagnetic waves to connect with a communication tower. When the communication between the cell phone antenna and the tower is good, the transmission power of the cell phone antenna is approximately 0.1 W. When the communication between the cell phone and the tower is poor, such as when the cell phone is inside an elevator or beneath a thick concrete building, or in a rural area, more transmission power is needed and this is emitted from the cell phone. The radiation rate at different antenna transmission power level is computed and presented in Fig. 9. It can be inferred that higher transmission power will be accompanied by higher rates of radiation.

8. Results on the thermal effects

In this section, the temperature rise from short-term and long-term exposures are discussed. Body temperature before being exposed to the electromagnetic wave is assumed as 37 °C. The heating effect on the human body is related to the thermal parameters of the tissue layers and the SAR.

8.1. Short-term exposure results

For the short-term temperature rise, SAR results from Section 6 are used as input for the bio-heat equation. As mentioned in Section 6, the 8 ns exposure time is very short, and the temperature rise during short-term exposure is directly related to the SAR results, and the distribution of the temperature rise and SAR are almost the same shape. For the 8 ns exposure time, the temperature rise for the TM wave is approximately 4.7×10^{-5} °C as shown in Fig. 10. For the 8 ns exposure time, the temperature rise for the TE wave is approximately 7.8×10^{-3} °C, as shown in Fig. 11. Thus, the temperature rise for the TM wave is much less than that for the TE wave.

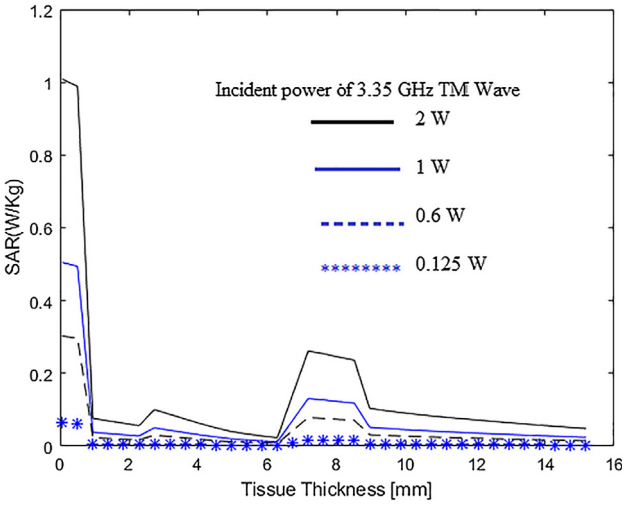

Fig. 9. Comparison of SAR with the incident source of the antenna.

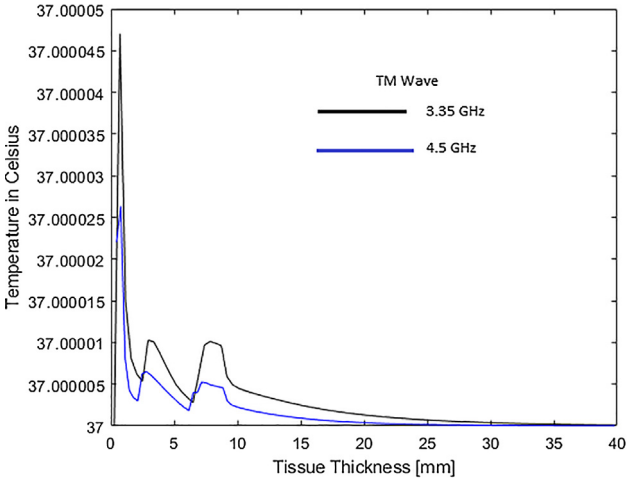

Fig. 10. Short-term heat transfer in the TM wave.

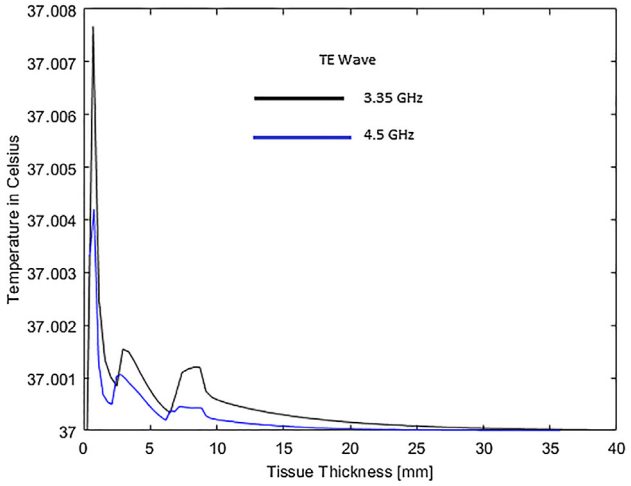

Fig. 11. Short-term heat transfer in the TE wave.

8.2. Long-term exposure result

Most people use the cell phone more for internet browsing than for conversation on a daily basis. Thus, for cases of long-term exposure, the effects of an incident power of 0.125 W was studied. According to the temperature rise results for long-term exposure, the transfer of heat depends not only on the SAR but also on the thermal parameters of the tissue layers, such as the blood flow. As shown in Fig. 12, the outer layers of tissue up to 10 mm, experienced a gradual temperature rise which then gradually decreases inside the head. It is noticeable that the SAR in the fat and bone layers is not much, but the temperature rise in those layers are more than in the skin layer, as shown in Fig. 13. Therefore, the SAR value is not directly affected by the computation of the thermal effects. The reasons for this situation are the heat transfer behavior and the blood flow constants of tissues presented in Table 2.

Even though the SAR in the skin layer is the highest, the temperature rise is less than in subsequent layers, such as fat and bone. The skin's blood flow parameter (b) is quite high, as shown in Table 1, and it means that there is blood flow in the skin layer. Increased blood flow would reduce the heat and also the skin is the outermost layer that can have its outside surface cooled by

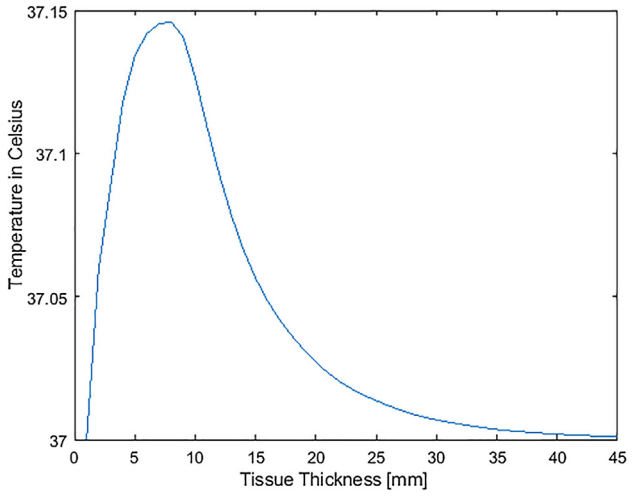

Fig. 12. Long-term heat transfer inside the human head.

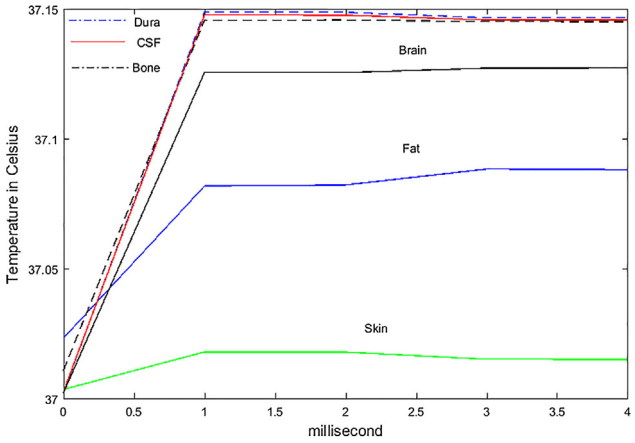

Fig. 13. Long-term heat transfer in each tissue layer.

the air and thus lower the heating rate. For the bone layer, the blood flow rate is lower than in any other tissue layer and there is no chance to reduce the heating. The CSF does not have any blood flow but is itself a type of fluid. Thus, the heating gradually declines from the dura to the inside of the brain. In comparison, the thermal effect of 8 ns exposure to 3.35 GHz TE wave of 1 W incident power, 1 cm distance from the source and 0.44 mm cell size (results in Fig. 11) is much less than the temperature rise from 3.35 GHz TE wave for 4 ms exposure with 0.125 W incident power, 0.5 cm distance from the source and 1 mm cell size (Fig. 12).

According to the information in Fig. 13, the maximum temperature in each tissue layer significantly increases until one millisecond. After that, it reaches a steady state. It is clear that the temperature in the skin is the lowest among the six tissue layers. The temperature reaches its peak at the Dura. The part of the brain region nearest to the source has a high temperature and farther from the source the temperature drops almost to the baseline temperature. However, the highest temperature in the brain region remains higher than that in the fat layer.

The simulation was done using MATLAB Software on a desktop computer with Intel (R) Xeon (R) CPU 3.33 GHz processor, and 48 GB RAM. The execution time for 8 ns exposure for 3.35 GHz and 4.5 GHz frequencies were approximately 1.5 min and 3 min respectively.

9. Conclusion

Using numerical calculation, we examined radiation effects such as SAR and temperature rise inside the human head. The FDTD method, SAR equation, and the bio-heat equation were used to calculate these effects. The electric field absorbed by the human body was determined using the calculations of the FDTD method, from which SAR was computed using the SAR equation. Temperature rise was computed from the SAR using the bio-heat equation. The simplest structure of the head model was used to obtain general information on the human tissue numerically. In the numerical computation technique, some fundamental parameters are important, and these can change the main output of the system. Thus, different types of FDTD parameters and possible situations of the radiation source related properties were also studied and highlighted.

According to the results for short-term exposure, SAR and the temperature distribution are closely related. When we use the cell phone for a long time, the SAR distribution is different from the temperature distribution because of the nature of the heat transfer. The distribution of temperature rise for longer exposures depends on the thermal parameters of the tissue. The effects of long-term exposure are emphasized in this study because of the cell phone usage habit in the modern world. The simulation was implemented using MATLAB code. To get the long exposure results, a great number of FDTD iterations were needed because the spatial time step (picoseconds) is too small. To get a faster processing time, the MATLAB MEX function was used. To calculate for long exposures, a high-performance computer is needed. The two-dimensional approach was used for the simulations to be cost-effective concerning hardware cost and execution time. However, it is necessary to prove the reliability of the two-dimensional results by comparing with the results of a three-dimensional calculation. The three-dimensional based calculation and other types of transmission source have been earmarked for future study.

References

[1] Bhat MA, Kumar V. Calculation of SAR and measurement of temperature change of human head due to the mobile phone waves at frequencies 900 MHz and 1800 MHz. Adv Phys Theories Appl 2013;16:54–63.
[2] Siriwitpreecha A, Rattanadecho P, Wessapan T. The influence of wave propagation mode on specific absorption rate and heat transfer in human body exposed to electromagnetic wave. Int J Heat Mass Transf 2013;65:423–34.
[3] Shiba K, Higaki N. Analysis of SAR and current density in human tissue surrounding an energy transmitting coil for a wireless capsule endoscope. In: 2009 20th International Zurich symposium on electromagnetic compatibility, Zurich. p. 321–4.
[4] Wang J, Fujiwara O. FDTD computation of temperature rise in the human head for portable telephones. IEEE Trans Microw Theory Tech 1999;47(8):1528–34.
[5] Hirata A, Shirai K, Fujiwara O. On averaging mass of SAR correlating with temperature elevation due to a dipole antenna. Progress in Electromag Res, PIER 2008;84:221–37.
[6] Vaquer M, Mallorqui JJ, Cardama A, Jofre U. Bidimensional scattering of TM and TE polarized waves by dielectric bodies using the CG-FFT method: application to mobile communication systems. In: Proc. of the 23rd EMC. p. 409–11.
[7] Ohishi Takifumi, Haji Yuki, Tokumara Shinobu. Incident angle characteristic of SAR in two- dimensional three-layered ellipse human model exposed to EM plane waves. Electron Commun Japan, Part 1 2002;85(12).
[8] Nishizawa S, Hashimoto O. Effectiveness analysis of lossy dielectric shields for a three-layered human model. IEEE Tranfs Microwave Theory Tech. 1999;47 (3):277–86.
[9] Alisoy HZ. An FDTD based numerical analysis of microwave propagation properties in a skin-fat tissue layers. Optik J 2013;124(21):5218–24.
[10] Khodabakhshi H, Cheldavi A. Irradiation of a six-layered spherical model of human head in the near field of a half-wave dipole antenna. IEEE Trans Microw Theory Tech 2010;58(3):680–90.
[11] Taflove A, Hagness SC. Computational Electrodynamics: the finite-difference time-domain method. USA: Artech House; 2000.
[12] Ishimaru. Electromagnetic wave propagation, radiation, and scattering. 2nd Ed. UK: IEEE Press; 2017.
[13] Andreuccetti D, Fossi R, Petrucci C. An Internet resource for the calculation of the dielectric properties of body tissues in the frequency range 10 Hz – 100

GHz. Website at <http://niremf.ifac.cnr.it/tissprop/>. IFAC-CNR, Florence (Italy), 1997. Based on data published by C. Gabriel et al. 1996.
[14] Sabbah AI, Dib NI, Al-Nimr MA. SAR and temperature elevation in a multi-layered human head model due to an obliquely incident plane wave. Progress Electromag Res M 2010;13:95–108. https://doi.org/10.2528/PIERM10051502.
[15] Omar AA, Bashayreh QM, Al-Shamali AM. Investigation of the effect of obliquely incident plane wave on a human head at 900MHz and 1800 MHz. Int J RF Microwave CAE March 2010;20(2):133–40.
[16] International commission on non-ionizing radiation protection ICNIRP guidelines for limiting exposure to time-varying electric, magnetic and electromagnetic fields (up to 300 GHz), published in Health Physic 1998;74 (4):494–522.
[17] IEEE C95.1.IEEE standard for safety levels with respect to human exposure to radio frequency electromagnetic fields, 3kHz to 300 GHz. IEEE Std C95.1-2005.
[18] Kamalaveni A, Ganesh Madhan M. A compact TRM antenna with high impedance surface for SAR reduction at 1800 MHz. Int J Electron Commun (AEÜ) 2016;70:1192–8.